Systemic Biodistribution and Intravitreal Pharmacokinetic Properties of Bevacizumab, Ranibizumab, and Aflibercept in a Nonhuman Primate Model

John Byron Christoforidis,[1,2] Karen Briley,[3] Katherine Binzel,[3] Prayna Bhatia,[3] Lai Wei,[4] Krishan Kumar,[3] and Michael Vinzenz Knopp[3]

[1]Department of Ophthalmology & Vision Science, University of Arizona Medical Center, Tucson, Arizona, United States
[2]Retina Specialists of Southern Arizona, Tucson, Arizona, United States
[3]Department of Radiology, College of Medicine, The Ohio State University, Columbus, Ohio, United States
[4]Center for Biostatistics, College of Medicine, The Ohio State University, Columbus, Ohio, United States

Correspondence: John Byron Christoforidis, Department of Ophthalmology & Visual Science, University of Arizona Medical Center, 655 N. Alvernon Way, Suite 108, Tucson, AZ 85711, USA; jbchristo@hotmail.com.

Submitted: June 14, 2017
Accepted: September 30, 2017

Citation: Christoforidis JB, Briley K, Binzel K, et al. Systemic biodistribution and intravitreal pharmacokinetic properties of bevacizumab, ranibizumab, and aflibercept in a nonhuman primate model. *Invest Ophthalmol Vis Sci*. 2017;58:5636–5645. DOI: 10.1167/iovs.17-22431

Purpose. To determine the intravitreal pharmacokinetic properties and to study the systemic biodistribution characteristics of I-124-labeled bevacizumab, ranibizumab, and aflibercept with positron emission tomography–computed tomography (PET/CT) imaging in a nonhuman primate model.

Methods. Three groups with four owl monkeys per group underwent intravitreal injection with 1.25 mg/0.05 mL I-124 bevacizumab, 0.5 mg/0.05 mL I-124 ranibizumab, or 2.0 mg/0.05 mL I-124 aflibercept in the right eye of each subject. All subjects were imaged using PET/CT on days 0, 1, 2, 4, 8, 14, 21, 28, and 35. Serum blood draws were performed at hours 1, 2, 4, 8, 12 and days 1, 2, 4, 8, 14, 21, 28, and 35. Radioactivity emission measurements were used to determine the intravitreal half-lives of each agent and to study the differences of radioactivity uptake in nonocular organs.

Results. The intravitreal half-lives were 3.60 days for I-124 bevacizumab, 2.73 days for I-124 ranibizumab, and 2.44 days for I-124 aflibercept. Serum levels were highest and most prolonged for bevacizumab as compared to both ranibizumab and aflibercept. All agents were primarily excreted through the renal and mononuclear phagocyte systems. However, bevacizumab was also found in significantly higher levels in the liver, heart, and distal femur bones.

Conclusions. Among the three anti-VEGF agents used in clinical practice, bevacizumab demonstrated the longest intravitreal retention time and aflibercept the shortest. Significantly higher and prolonged levels of bevacizumab were found in the serum as well as in the heart, liver, and distal bones. These differences may be considered by clinicians when formulating treatment algorithms for intravitreal therapies with these agents.

Keywords: biodistribution, pharmacokinetics, radiolabeling, positron emission tomography, intravitreal drug delivery

Anti-vascular endothelial growth factor (VEGF) agents such as bevacizumab (Avastin; Roche, Basel, Switzerland), ranibizumab (Lucentis; Roche), and aflibercept (Eylea; Regeneron, Tarrytown, NY, USA) have become the treatments of choice in the pharmacologic treatment of retinal neovascular disorders such as the exudative form of macular degeneration, macular edema from diabetic retinopathy and venous occlusions, and retinopathy of prematurity. Since their inception in 2005, the number of anti-VEGF injections in the United States has increased 10% to 20% annually.[1] Intravitreal injection therapy of these agents is now the most commonly performed procedure in ophthalmology, and it is estimated that over 6 million injections were performed in the United States in 2016 alone.[2]

The intravitreal anti-VEGF drugs in clinical use today are clear substances that cannot be visualized following injection. Radiolabeling these agents allows them to be imaged through their radioactive emission with positron emission tomography (PET) imaging. Compared to immunoassay methods, positron emission tomography–computed tomography (PET/CT) allows the radiolabeled agents to be noninvasively visualized, and their radioactive emission permits the study of their pharmacokinetic and biodistribution properties. With seven to nine time points obtained per subject, a smaller number of subjects can be studied per treatment group to determine the pharmacokinetic characteristics of the therapeutic agent.

Previous reports on a rabbit model have successfully demonstrated that PET/CT can visualize I-124 bevacizumab, I-124 ranibizumab, and I-124 aflibercept in the vitreous cavity and can determine their pharmacokinetic properties.[3–5] In these previous studies, the intravitreal half-lives for bevacizumab and ranibizumab were 4.2 and 2.8 days, respectively, comparing favorably with previous reports using immunoassay methodologies in a similar rabbit model.[6–7]

Systemic biodistribution following systemic administration of I-124-radiolabeled agents has been previously reported.[8–10]

However, to our knowledge, the systemic biodistribution of intravitreally placed therapeutic agents has not been previously examined. Recent advances in PET technology have significantly improved image resolution and allowed for more precise quantification of radioactive emission measurements of tagged agents. This has improved our ability to more accurately determine their intravitreal pharmacokinetic characteristics and to track their dissemination into extraocular organs. The nonhuman primate (NHP) model has inherent advantages over previously used rabbit models including a human-like proportioned vitreous cavity and lens, and the presence of a macula critical for binocular vision and stereopsis. These anatomic similarities can provide a more accurate assessment of intravitreally placed drugs for human use.

In this project, we used high-resolution digital PET/CT (dPET/CT) to study the intravitreal pharmacokinetic properties and systemic biodistribution characteristics of I-124-labeled bevacizumab, ranibizumab, and aflibercept after intravitreal placement in a NHP model. The goals of our project were 3-fold: first, to determine the intravitreal pharmacokinetic properties of the three anti-VEGF agents by serial ocular imaging; second, to study the serum levels for each of the three agents after intravitreal injection; and third, to examine the systemic biodistribution of each agent by sequential whole-body PET.

Materials and Methods

Radiolabeling of bevacizumab, ranibizumab, and aflibercept with I-124 (IBA Molecular, Dulles, VA, USA) was completed using a modified Iodogen method.[11] Radiochemical purities for I-124 bevacizumab, I-124 ranibizumab, and I-124 aflibercept were 96.2%, 96.2%, and 96.6%, respectively.

All treatments were conducted in agreement with the ARVO Statement for the Use of Animals in Ophthalmic and Vision Research. All experimental protocols were approved, and the procedures followed were in accordance with the ethical standards of the Institutional Animal Care and Use Committee (IACUC) at The Ohio State University. Twelve (7 male and 5 female) adult *Aotus trivirgatus* known as owl monkeys (Keeling Center for Comparative Medicine and Research at The University of Texas MD Anderson Cancer Center, Bastrop, TX, USA) weighing 940 to 1150 g were used for this study. Under general anesthesia, three groups of 4 owl monkeys each underwent intravitreal injection. 1.25 mg/0.05 mL I-124 bevacizumab (2 female, 2 male), 0.5 mg/0.05 mL I-124 ranibizumab (2 female, 2 male), or 2.0 mg/0.05 mL I-124 aflibercept (1 female, 3 male) was placed 1.5 mm posterior to the limbus using a 32-gauge needle in the right eye of each of the 12 subjects.

Immediately following intravitreal injection on day 0, each subject underwent dPET/CT imaging (Vereos; Philips Healthcare, Andover, MA, USA), and sequential imaging was performed on days 1, 2, 4, 8, 14, 21, 28, and 35. At each time point, two bed position acquisitions to cover the head and body of the NHPs were obtained. All dPET images were reconstructed using 2-mm voxel length. Serum was collected at postintravitreal injection hours 1, 2, 4, 8, and 12 and days 1, 2, 4, 8, 14, 21, 28, and 35. Between 1.0 and 1.5 mL blood from the femoral artery was collected in BD Vacutainer Plus plastic serum tubes with 5.0-mL Gold BD Hemogard closure venous blood collection tubes (BD, Franklin Lakes, NJ, USA). Radioactive emission levels from the collected blood samples were then measured with a gamma counter (WIZARD2 Automatic Gamma Counter; Perkin Elmer, Inc., Waltham, MA, USA). The collected blood was then centrifuged at 1000*g* for 5 minutes (Eppendorf 5415C, Eppendorf North America, Nauppauge, NY, USA), and the separated serum was collected using 7-mL polyethylene LabAid transfer pipettes (Biomed Resource, Inc., Riverside, CA, USA) and placed into polypropylene 1.5-mL tubes (Heathrow Scientific LLC, Vernon Hill, IL, USA). At the completion of the study, the subjects were quarantined to allow for 10 half-lives of I-124 radioactivity decay following intravitreal injection (42 days or 1 week after the last imaging session) before being released.

The radioactive units (Bq/mL) were corrected to account for I-124 radioactive decay, which has a physical half-life of 4.18 days. Clearance curves were then formulated with the resulting measurements, and the intravitreal half-life for each subject was calculated using a formula to describe first-order kinetics:

$$T_{1/2} = \frac{T \times \log 2}{\log [\text{Drug}]_b / [\text{Drug}]_e}$$

Whereby: $T_{½}$ = Half-Life
T = Elapsed Time
$[\text{Drug}]_b$ = Beginning Amount
$[\text{Drug}]_e$ = Ending Amount

To study the biodistribution patterns of each agent after intravitreal injection, PET/CT images of specific organs were examined. In addition to the injected right eye, 11 other organs that exhibited radioactive uptake were examined and compared for each of the three agents. The examined organs were the contralateral left eye, right and left thyroid lobes, right and left kidneys, bladder, spleen, right and left distal femur bones, heart, and liver. The regions of interest (ROI) for each tissue type were held constant for all imaging sessions, and all analysis was performed using Philips Healthcare software. Mean standardized uptake values (SUV) values were determined as a function of postinjection time for each antibody tested. The SUV scales were adjusted to lower emission thresholds to allow for better visualization of organs with lower radioactivity levels.

Statistical analysis was performed to compare differences in the three treatment groups with 1-way analysis of variance (ANOVA) with post hoc Tukey honest significant difference (HSD) test for multiple comparisons to adjust for multiple hypothesis tests, and statistical significance was set at $P < 0.05$. Means and standard errors were calculated for each treatment at each time. All analyses were performed using SAS/STAT software, Version 9.4 (SAS Institute, Inc., Cary, NC, USA).

Results

Intravitreal Anatomic and Pharmacokinetic Properties

During the course of the study, none of the eyes developed adverse events such as endophthalmitis, uveitis, or cataract. The montage in Figure 1 illustrates serial images for three subjects, one for each of the three agents. I-124 bevacizumab was visible until day 21 while both I-124 ranibizumab and I-124 aflibercept were visible until day 14. Intravitreal levels of radioactivity (Bq/mL) are listed for each subject in Table 1. I-124 uptake in the thyroid lobules was visible on day 35 in all subjects, indicating that the radioactivity clearance from the vitreous cavity was due to agent egress from the vitreous rather than I-124 radioactive decay.

The resulting clearance patterns for each agent fit a two-phase curve with an initial rapid distribution phase until day 4 followed by a slower elimination phase from day 8 onward (Fig. 2). By graphic extrapolation of I-124 levels to the noise

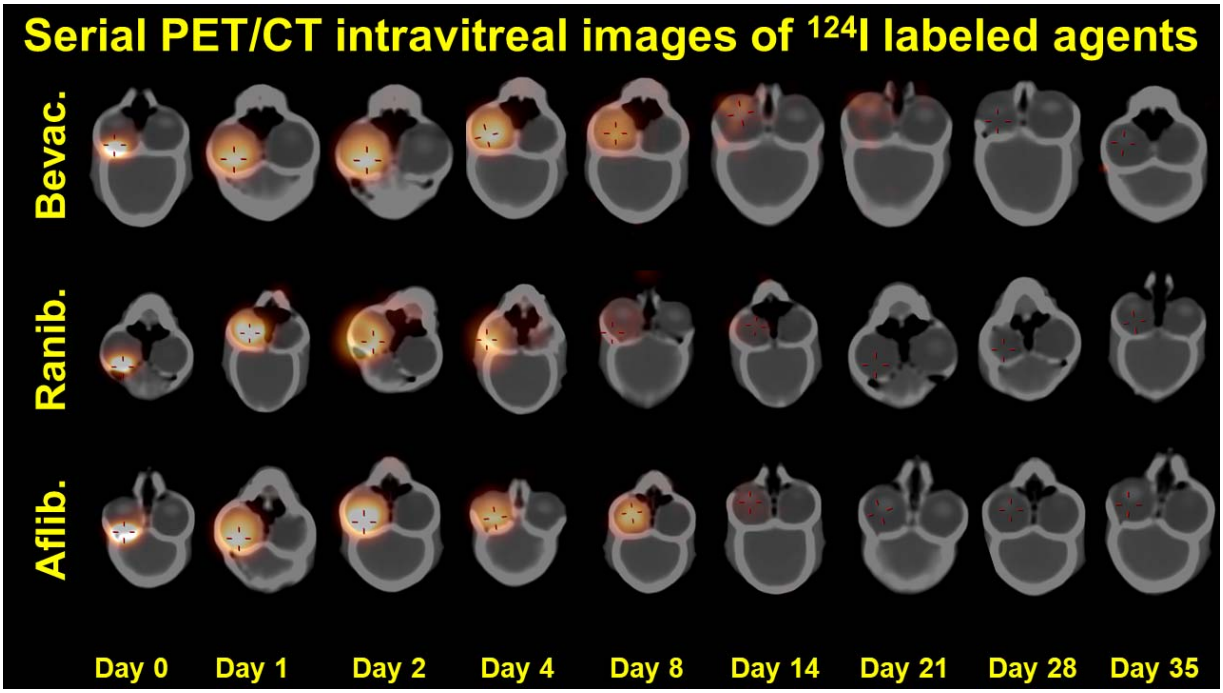

Figure 1. Serial image montage illustrating clearance patterns of I-124 bevacizumab (*top*), I-124 ranibizumab (*middle*), and I-124 aflibercept (*bottom*) in an owl monkey model. I-124 bevacizumab was discernible until day 21 and detectable until day 28, while I-124 ranibizumab and I-124 aflibercept were visible until day 14 and detectable until day 21.

plane, average I-124 bevacizumab was detectable in the vitreous cavity until day 30, average I-124 ranibizumab until day 22, and average I-124 aflibercept until day 21. The average clearance half-lives with standard error and 95% confidence intervals after correction for radioactive decay were found to be 3.60 ± 0.20 (3.40, 3.79) days for bevacizumab, 2.73 ± 0.19 (2.55, 2.92) days for ranibizumab, and 2.44 ± 0.32 (2.12, 2.76) days for aflibercept. The difference was significantly higher for I-124 bevacizumab than for both other agents ($P < 0.05$), and the calculated half-lives were not significantly different between ranibizumab and aflibercept.

The drug retention rates were found to trend higher for the females in each of the agent groups. The average intravitreal half-lives were 3.73 days for females and 3.46 days for males in the I-124 bevacizumab group, 2.97 days for females and 2.49 days for males in the I-124 ranibizumab group, and 3.16 days for the single female and 2.12 days for the three males in the I-124 aflibercept group. The number of subjects per male and female group was too small for statistical considerations.

Drug Serum Levels

Table 2 lists the mean measured serum I-124 bevacizumab, I-124 aflibercept, and I-124 ranibizumab levels with standard errors in gamma counter radioactivity counts at each time point. The values are graphically represented in Figure 3. There were no significant differences between the three drug levels up to 4 hours post intravitreal injection. Beginning at 8 hours post injection, I-124 bevacizumab levels measured significantly higher than the other two agents, and they remained significant compared to both agents for the remainder of the study. No significant differences in the serum levels were found between I-124 aflibercept and I-124 ranibizumab at any of the measured time points. I-124 ranibizumab levels were measurable until day 4 and I-124 aflibercept until day 8, and both were compatible with background noise thereafter.

Table 3 summarizes the pharmacokinetic parameters for each treatment group. The average peak serum concentration (C_{max}) was highest for the I-124 bevacizumab subjects (7.80 ± 1.75 ng/mL), lower for I-124 aflibercept (3.50 ± 0.31 ng/mL),

Table 1. Intravitreal Radioactivity Levels (Bq/mL)

Sex	F	M	F	M	F	M	F	M	F	M	M	M
Day	Lucentis	Lucentis	Lucentis	Lucentis	Avastin	Avastin	Avastin	Avastin	Eylea	Eylea	Eylea	Eylea
0	1238176	2226348	1544988	2361806	4924195	5238554	1853140	2895941	1575156	1098949	1119739	1225421
1	910799	510882	630789	320859	1568718	996153	1441724	1541633	1071211	518112	608523	676933
2	430081	186467	305297	103681	851048	496990	762783	912302	399504	238891	194961	483031
4	65708	27162	37218	16983	260490	129286	163401	217691	109959	49172.2	14254.5	109452
8	8633	1638	3575	1230	21918	9910	15320	13752	9356	3072	2866	10317
14	456	238	222	111	1339	1043	963	1803	290	72	295	364
21	82	45	44	13	249	137	404	161	51	4	46	15
28	30	16	13	5	52	28	144	50	34	0	1	12
35	3	2	0	0	13	6	1	15	0	0	0	0

Listing of intravitreal radioactivity levels (Bq/mL) for each of the three agents at each time point. Radioactivity levels below 30 Bq/mL were considered to be compatible with background noise.

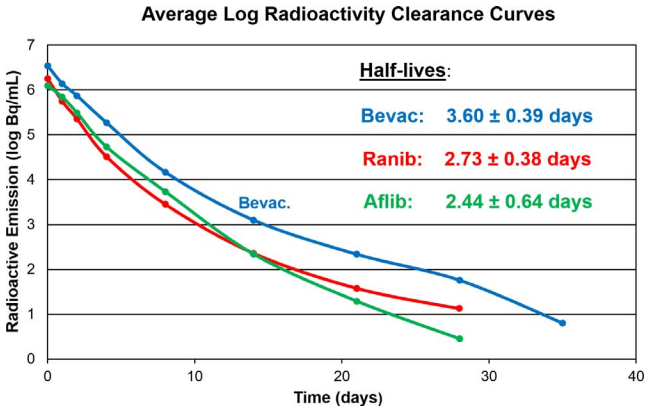

FIGURE 2. Summary of the average logarithmic clearance curves of I-124-labeled aflibercept (*green*), bevacizumab (*blue*), and ranibizumab (*red*). I-124 bevacizumab had the longest half-life while I-124 aflibercept had the shortest.

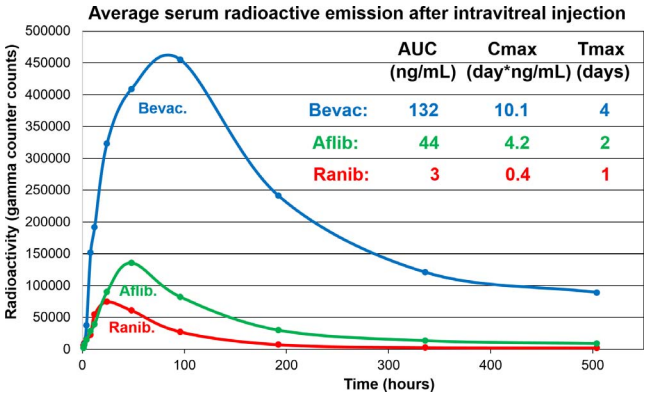

FIGURE 3. Graphic representation of average serum clearance curves of I-124-labeled aflibercept (*green*), bevacizumab (*blue*), and ranibizumab (*red*). I-124 bevacizumab had significantly larger AUC, C_{max}, and T_{max} when compared to the other two agents. There were no significant differences in the serum levels between I-124 aflibercept and I-124 ranibizumab at any of the measured time points.

and least for I-124 ranibizumab (0.47 ± 0.07 ng/mL). These differences were significantly higher for I-124 bevacizumab serum levels than for both I-124 aflibercept and I-124 ranibizumab ($P = 0.038$ and $P = 0.002$, respectively), but they were not significantly higher for I-124 aflibercept when compared to I-124 ranibizumab ($P = 0.147$).

The average time to maximal plasma concentration (T_{max}) was earliest for the I-124 ranibizumab (24 hours), followed by I-124 aflibercept (48 hours) and I-124 bevacizumab (84 hours). The area under the curve (AUC) was greatest for I-124 bevacizumab (109.0 ± 17.51 day*ng/mL) followed by I-124 aflibercept (38.63 ± 3.76 day*ng/mL) and I-124 ranibizumab (2.79 ± 0.55 day*ng/mL). AUC was significantly higher for I-124 bevacizumab than for both I-124 aflibercept and I-124 ranibizumab ($P = 0.002$ and $P < 0.001$, respectively). The higher AUC for I-124 aflibercept compared to I-124 ranibizumab was not significant ($P = 0.085$).

Systemic Biodistribution

Figure 4 demonstrates three PET/CT montages for one subject from each of the three treatment groups, and Figure 5 is a magnified view of an I-124 bevacizumab subject on day 4 depicting the various organs with radioactivity uptake following intravitreal injection in greater detail. Figures 6 through 8 graphically represent the differences in biodistribution findings for each of the examined organs. Table 4 summarizes the *P* values adjusted for multiple comparisons between the three treatment groups at each time point and for each studied organ.

Radioactivity levels were not measurable in any of the organs after day 21, with the exception of the injected right eye and both thyroid lobules. Radioactivity measurements in the studied bilateral extraocular organs (thyroid, kidneys, and distal femurs) revealed close correlation between the left and right sides at each time point. In general, I-124 bevacizumab was present in extraocular organs at higher levels in the later time points and was found to be significantly more disseminated in these organs compared to the other two agents. I-124 aflibercept and I-124 ranibizumab exhibited similar biodistribution patterns and were primarily found at earlier time points in excretory organs such as the urinary system (kidneys and bladder) and mononuclear phagocytic system (MPS, spleen). There was no accumulation found in the central nervous system for any of the labeled agents, and there were no significant differences or trends found in the biodistribution of any of the studied extraocular organs between male and female subjects.

Injected and Contralateral Eye (Fig. 6). The injected right eyes did not display significant differences between the three labeled drugs during the first week after injection (days 0–8). Beginning on day 14, I-124 bevacizumab was found in

TABLE 2. Labeled Agent Serum Level Means With Standard Errors and Statistical Comparisons

Hour	I-124 Bevacizumab	I-124 Aflibercept	I-124 Ranibizumab	*P* Value, Bev vs. Afl	*P* Value, Bev vs. Ran	*P* Value, Afl vs. Ran
1	2647 ± 636	2443 ± 607	6163 ± 1733	0.991	0.122	0.100
2	7886 ± 1726	6694 ± 1344	9559 ± 906	0.815	0.674	0.344
4	37902 ± 12609	14826 ± 2048	16272 ± 3389	0.137	0.167	0.990
8	151810 ± 24126	28266 ± 3290	22636 ± 5922	<0.001	<0.001	0.959
12	192031 ± 12975	39266 ± 1090	54758 ± 11112	<0.001	<0.001	0.533
24	323202 ± 31799	90061 ± 10750	74466 ± 11561	<0.001	<0.001	0.855
48	409142 ± 29377	135845 ± 13826	60965 ± 8551	<0.001	<0.001	0.055
96	455267 ± 69745	82321 ± 13173	27103 ± 8368	<0.001	<0.001	0.623
192	241397 ± 31434	30209 ± 3222	7084 ± 1655	<0.001	<0.001	0.657
336	120908 ± 22026	13693 ± 2712	2585 ± 702	<0.001	<0.001	0.817
504	89300 ± 94328	9066 ± 1660	2006 ± 422	<0.001	<0.001	0.867

Comparison of mean serum I-124 bevacizumab (Bev), I-124 aflibercept (Afl), and I-124 ranibizumab (Ran) levels with standard errors (gamma counter counts) at each measured time point. Adjusted *P* values for multiple comparisons reflect significant differences between I-124 bevacizumab and both other agents beginning at 8 hours post injection. There were no significant differences in the serum levels between I-124 aflibercept and I-124 ranibizumab at any of the measured time points.

Table 3. Pharmacokinetic Parameter Means With SD for Each Treatment Group

Parameter	I-124 Bev	I-124 Afl	I-124 Ran	*P* Value, Bev vs. Afl	*P* Value, Bev vs. Ran	*P* Value, Afl vs. Ran
T_{max}, h	84 ± 12	24 ± 0	48 ± 0	0.013*	0.001*	0.085
C_{max}, ng/mL	7.80 ± 1.75	3.50 ± 0.31	0.47 ± 0.07	0.038*	0.002*	0.147
AUC, day*ng/mL	109.0 ± 17.51	38.63 ± 3.76	2.79 ± 0.55	0.002*	0.001*	0.085

Listing of mean serum pharmacokinetic parameters with standard errors for the I-124 bevacizumab (Bev), I-124 aflibercept (Afl), and I-124 ranibizumab (Ran) groups. *P* values were adjusted for multiple comparisons with $P < 0.05$ set for statistical significance. The differences between I-124 bevacizumab and the other two agents were significant for T_{max}, C_{max}, and AUC, while there were no significant differences for any of the parameters between I-124 aflibercept and I-124 ranibizumab.

* Statistical significance ($P < 0.05$).

significantly higher levels compared to both other agents. In the noninjected left eyes, all three labeled agents were visible on days 1, 2, and 4. I-124 bevacizumab was significantly higher than both other agents only at day 8, and all agents had very low levels of detection after day 8.

Thyroid Gland (Fig. 6). Accumulation of I-124 in the thyroid gland was clearly visible at all of the time points beginning on day 1. No significant differences between the agents were found throughout the study. The three agents peaked at day 8, followed by gradually decreasing levels until day 35.

Urinary and Mononuclear Phagocytic Systems (Fig. 7). I-124 ranibizumab was found at significantly higher levels in both kidneys and the bladder on days 1 and 2 compared to both other agents. All three agents were clearly visible in the spleen on days 1, 2, and 4 without significant differences between them.

Other Organs (Fig. 8). I-124 bevacizumab was visible at levels that were significantly higher compared to both other labeled agents at all measurable time points in the heart, liver, and both distal femurs. For each of these organs, I-124 bevacizumab levels peaked at day 2 and then decreased gradually until disappearing after day 21.

Discussion

In this investigation, I-124 bevacizumab was found to have a significantly longer half-life (3.60 days) compared to the two other labeled agents. Ranibizumab had a longer half-life (2.73 days) than aflibercept (2.44 days) that was not significantly different. The half-lives of the three labeled anti-VEGF agents in this study were found to be shorter than those in previously published reports on a rabbit model.[4,12] This is likely due to the liquefied nature of the vitreous found in adult owl monkey eyes and is consistent with the significantly faster clearances found in postvitrectomized eyes in a rabbit model using similar PET methodology.[5,13] There is scant literature on pharmacokinetic studies examining intravitreal ranibizumab and aflibercept on a primate model. One recent report by Niwa et al.[14] studied serial aqueous humor drug measurements in macaques after intravitreal injections with ranibizumab and aflibercept, and the half-lives were found to be 2.3 days for ranibizumab and 2.2 days for aflibercept, more similar to our results.

I-124 bevacizumab serum levels and pharmacokinetic parameters were significantly higher than both other agents, and those of I-124 aflibercept were higher than those of I-124 ranibizumab. Gamma counter radioactivity levels rather than immunoassay methods were used to assess the labeled anti-

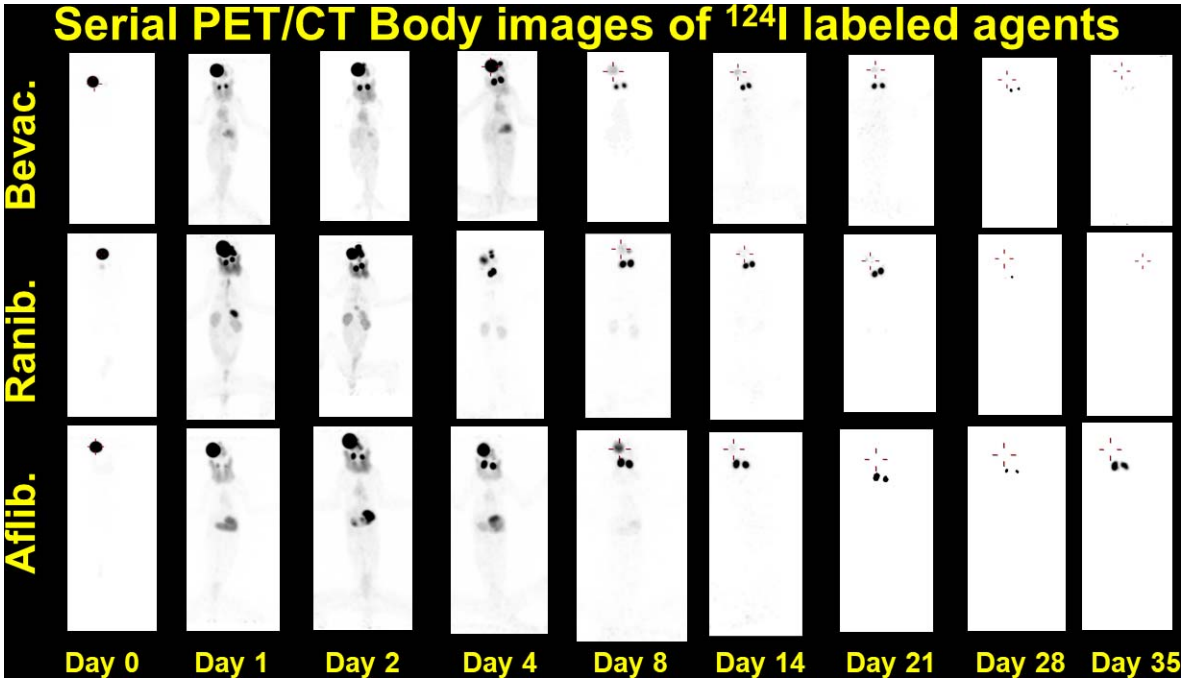

Figure 4. Serial image montage illustrating the systemic biodistribution of I-124 bevacizumab (*top*), I-124 ranibizumab (*middle*), and I-124 aflibercept (*bottom*) in an owl monkey. Accumulations in the injected eye and both thyroid lobules were seen throughout the study while radioactivity could be detected in other organs until day 21. I-124 bevacizumab had the widest and most prolonged biodistribution among the three agents.

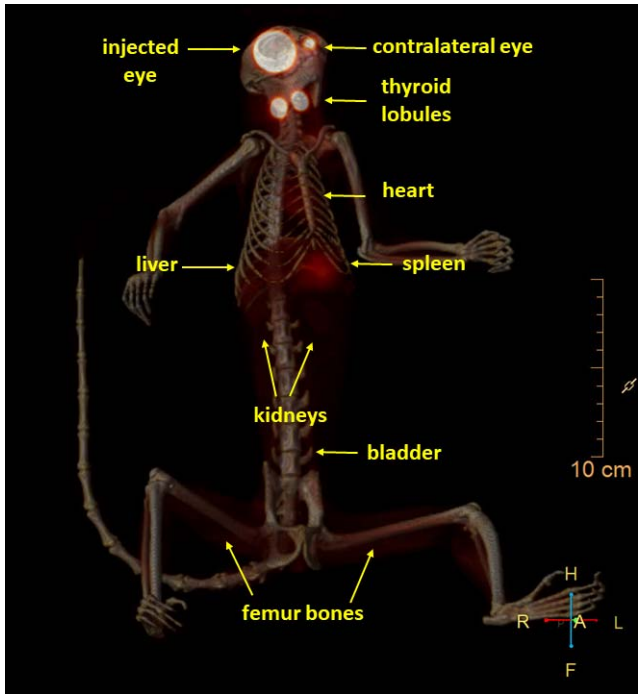

FIGURE 5. Magnified PET/CT image of an I-124 bevacizumab-treated subject on day 4 depicting radioactivity uptake in various organs following intravitreal injection.

VEGF agents in the serum. The trends in the serum found for each the three agents reflect differences similar to those reported by Avery et al.[15,16] in humans studying the same three agents.

Few studies have reported serum ranibizumab levels after intravitreal injection because they are either found at very low levels or are not measurable by 2 days after injection (Jiang A, et al. *IOVS* 2012;53:ARVO E-Abstract 2964; Christoforidis JB, et al. *IOVS* 2014;55:ARVO E-Abstract 1938).[7,17,18] To capture the earlier systemic clearance pattern previously reported for ranibizumab, this study included multiple early time points at 1, 2, 4, 8, and 12 hours after injection. The findings confirmed that after peaking in the serum 24 hours post injection, ranibizumab was rapidly cleared from the bloodstream. Previous studies have examined VEGF serum levels following intravitreal anti-VEGF injection and have reported shorter duration and less VEGF suppression in the serum after ranibizumab intravitreal placement in comparison to both bevacizumab and aflibercept.[15,16,19–21] Peripheral VEGF suppression has been found to be especially pronounced after intravitreal bevacizumab therapy in patients with retinopathy of prematurity.[22–24]

Bevacizumab and aflibercept have an Fc-fragment that allows the agents to be engulfed by RPE cells and retinal endothelial cells.[25,26] By contrast, ranibizumab lacks the Fc-fragment and is rapidly cleared from the circulation once the drug enters the bloodstream.[27] Internalization of the Fc-containing agents may allow their physiological effects to remain active after they are no longer detectable by PET imaging. It is uncertain whether the hybrid structure of aflibercept affects the duration of its intracellular captivity as reflected by the reduced half-lives within the vitreous and in the serum as compared to bevacizumab in this study and in other reports.[15,16,25]

The accumulation of anti-VEGF agents in extraocular organs after intravitreal injection has not been previously examined, and the clinical consequences of the dissemination patterns found in this study are uncertain. Previous studies on rabbits using the same methodology were performed using one bed acquisitions focusing on the head and neck.[3–5] Although significant radioactive accumulations were reported in those studies, radioactivity in other extraocular organs below the neck would not have been detected. In clinical practice, ophthalmologists are often not aware of a patient's ongoing medical history, and associations of systemic adverse events

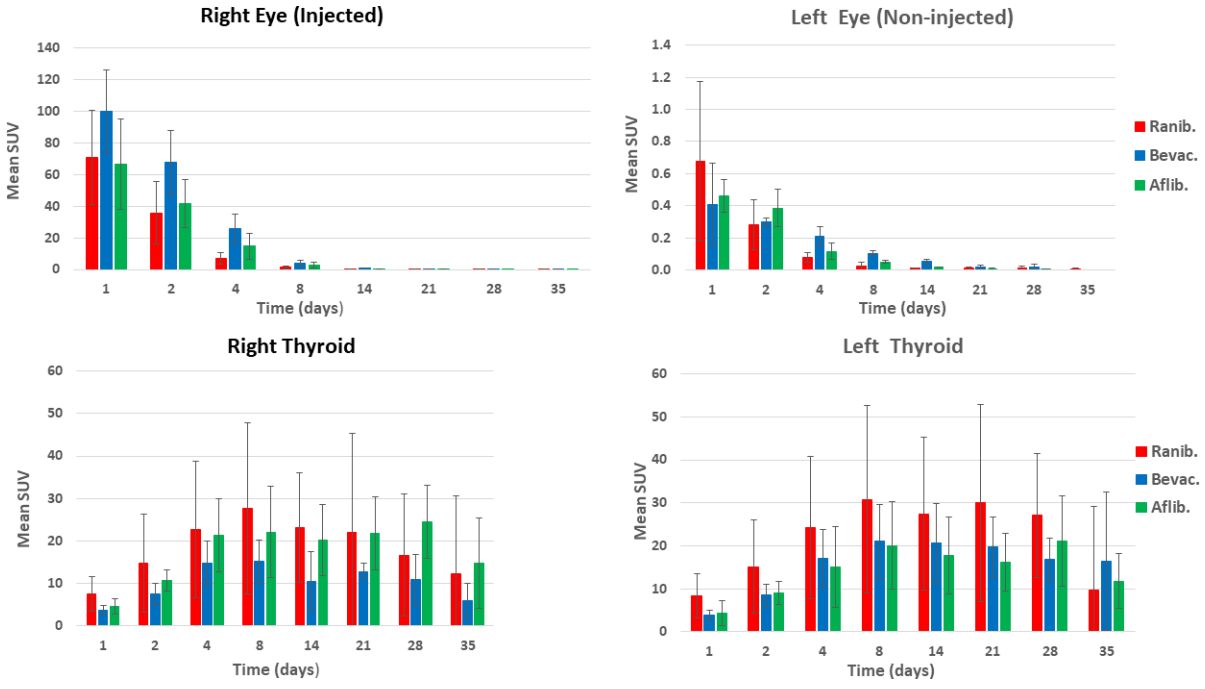

FIGURE 6. Comparison of serial radioactivity uptake values with standard error bars in mean standardized uptake values (SUV) between the three anti-VEGF agents in the injected and noninjected eyes, as well as thyroid lobules.

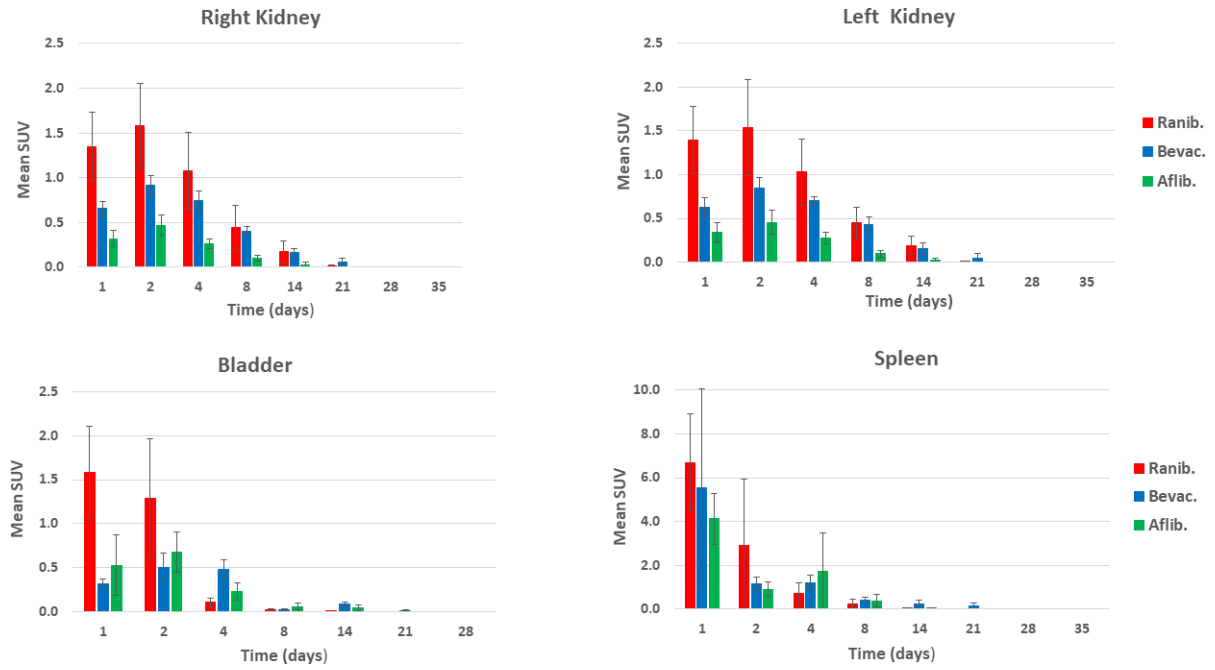

FIGURE 7. Comparison of serial radioactivity uptake values with standard error bars in mean standardized uptake values (SUV) between the three anti-VEGF agents in both kidneys, bladder, and spleen.

following intravitreal injection are likely to be underreported. The side effects of systemic bevacizumab are well known and include hypertension, proteinuria, wound dehiscence, incisional hernias, surgical site bleeding, gastrointestinal perforation, nonocular hemorrhages, and thromboembolic events.[28–33] Systemic side effects following intravitreal anti-VEGF therapy are less clear. A subset of patients including elderly patients, diabetics, and infants with retinopathy of prematurity (ROP) may be especially susceptible to systemic adverse events such as stroke, wound healing complications, and death.[34] A meta-analysis of Comparison of Age-related Macular Degeneration Treatments Trials (CATT) and Inhibition of VEGF in Age-related choroidal Neovascularisation (IVAN) clinical trials at the 2-year mark showed a significant increase in the risk of developing certain systemic side effects including gastrointestinal hemorrhages, hernias, nausea, and vomiting with bevacizumab when compared to ranibizumab.[35,36] In a rabbit model, intravitreally placed bevacizumab was found to significantly delay cutaneous wound healing in a rabbit model.[37] In the kidney, preglomerular, glomerular, and peritubular endothelial cells are known to

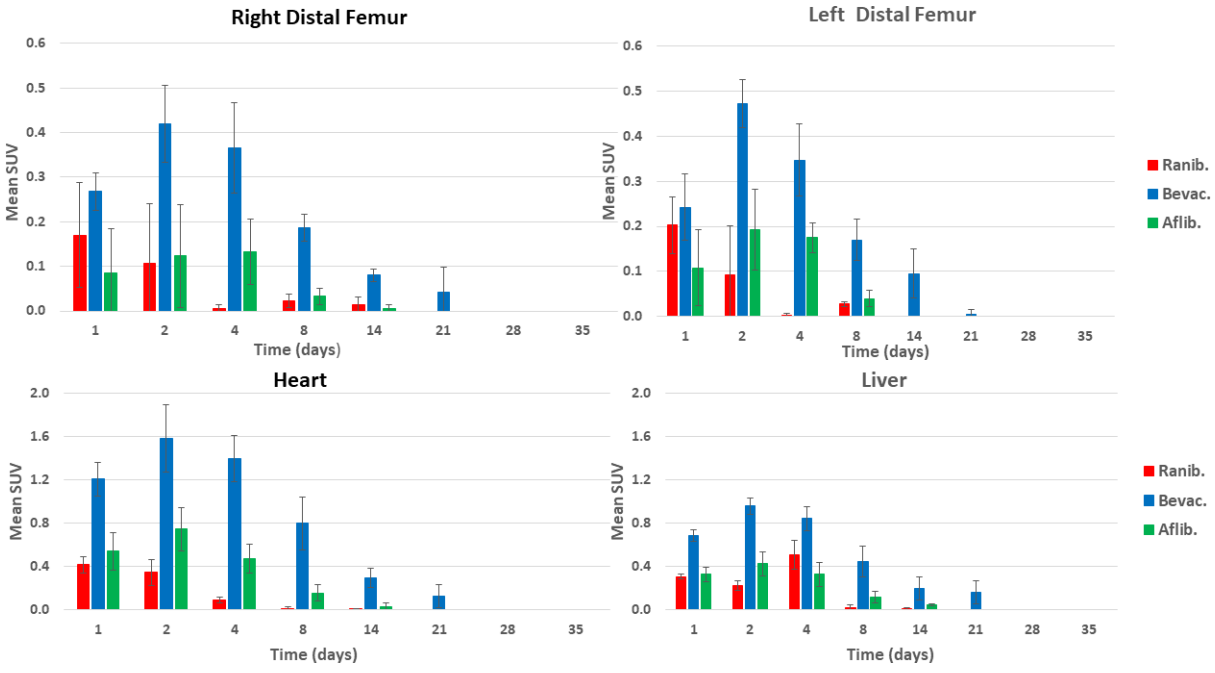

FIGURE 8. Comparison of serial radioactivity uptake values with standard error bars in mean standardized uptake values (SUV) between the three anti-VEGF agents in both distal femurs, heart, and liver.

Table 4. Statistical Summary Between the Three Treatment Groups

Organ	Comparison	Day 0	Day 1	Day 2	Day 4	Day 8	Day 14	Day 21	Day 28	Day 35
Right eye	Ran vs. Bev	0.546	0.360	0.084	0.015*	0.102	0.001*	0.037*	0.372	0.041*
	Ran vs. Afl	0.348	0.975	0.898	0.343	0.538	0.912	0.566	0.046*	0.842
	Bev vs. Afl	0.072	0.272	0.165	0.151	0.467	0.001*	0.007*	0.005*	0.017*
Left eye	Ran vs. Bev		0.499	0.974	0.022*	<0.001*	<0.001*	0.504	0.489	0.140
	Ran vs. Afl		0.636	0.443	0.569	0.131	0.365	0.921	0.659	0.140
	Bev vs. Afl		0.969	0.562	0.076	0.003*	0.003*	0.315	0.149	1.000
Right thyroid	Ran vs. Bev		0.145	0.338	0.581	0.424	0.214	0.650	0.719	0.766
	Ran vs. Afl		0.297	0.685	0.984	0.833	0.904	1.000	0.606	0.957
	Bev vs. Afl		0.871	0.798	0.682	0.752	0.380	0.666	0.258	0.602
Left thyroid	Ran vs. Bev		0.205	0.374	0.664	0.637	0.733	0.590	0.420	0.808
	Ran vs. Afl		0.266	0.423	0.533	0.579	0.550	0.399	0.758	0.970
	Bev vs. Afl		0.981	0.994	0.972	0.995	0.947	0.934	0.842	0.903
Right kidney	Ran vs. Bev		0.006*	0.025*	0.212	0.915	0.990	0.083		
	Ran vs. Afl		<0.001*	<0.001*	0.004*	0.023*	0.068	0.876		
	Bev vs. Afl		0.156	0.124	0.064	0.046*	0.084	0.039*		
Left kidney	Ran vs. Bev		0.006*	0.025*	0.212	0.915	0.990	0.083		
	Ran vs. Afl		<0.001*	<0.001*	0.004*	0.023*	0.068	0.876		
	Bev vs. Afl		0.156	0.124	0.064	0.046*	0.084	0.039*		
Spleen	Ran vs. Bev		0.852	0.410	0.800	0.558	0.024*	0.178		
	Ran vs. Afl		0.467	0.383	0.420	0.646	0.963	1.000		
	Bev vs. Afl		0.779	0.986	0.784	0.987	0.035*	0.178		
Bladder	Ran vs. Bev		0.014*	0.246	0.001*	0.997	0.040*	0.140		
	Ran vs. Afl		0.036*	0.413	0.183	0.273	0.434	1.000		
	Bev vs. Afl		0.827	0.970	0.010*	0.354	0.280	0.140		
Right femur	Ran vs. Bev		0.338	0.011*	<0.001*	<0.001*	0.001*	0.214		
	Ran vs. Afl		0.428	0.982	0.082	0.789	0.595	1.000		
	Bev vs. Afl		0.050	0.021*	<0.001*	<0.001*	<0.001*	0.214		
Left femur	Ran vs. Bev		0.734	<0.001*	<0.001*	<0.001*	0.005*	0.469		
	Ran vs. Afl		0.221	0.283	0.002*	0.777	1.000	1.000		
	Bev vs. Afl		0.071	0.004*	0.002*	<0.001*	0.005*	0.469		
Heart	Ran vs. Bev		<0.001*	<0.001*	<0.001*	<0.001*	<0.001*	0.063		
	Ran vs. Afl		0.459	0.078	0.013*	0.395	0.900	1.000		
	Bev vs. Afl		<0.001*	<0.001*	<0.001*	<0.001*	<0.001*	0.063		
Liver	Ran vs. Bev		<0.001*	<0.001*	0.008*	<0.001*	0.005*	0.073		
	Ran vs. Afl		0.846	0.017*	0.132	0.339	0.681	1.000		
	Bev. vs. Afl		<0.001*	<0.001*	<0.001*	<0.001*	0.016*	0.073		

Summary of the *P* values adjusted for multiple comparisons between the three treatment groups at each time point and for each studied organ. In general, I-124 ranibizumab (Ran) revealed significantly higher uptake in the renal system (kidneys and bladder) at the earlier time points (days 1 and 2). I-124 bevacizumab (Bev) exhibited significantly higher uptake than both other agents in the heart, liver, and distal femur bones throughout the study, and in the injected eye at the latter time points.

* Indicates statistical significance ($P < 0.05$); blanks indicate no measurable radioactivity.

be VEGF-reliant.[38] Several studies in the nephrology literature have reported the presence of renal complications following intravitreal anti-VEGF therapy, including proteinuria and hypertension.[39–41] Tschulakow et al.[27] found that aflibercept and ranibizumab were both detected within glomerular capillaries after a single intravitreal injection of these agents in a cynomolgus primate model. Their findings are consistent with the rapid accumulation of ranibizumab in the kidneys following intravitreal injection found in this investigation.

There were several limitations in this study. First, peripheral organ uptake of I-124-labeled drugs after intravitreal injection is expected to be higher than that measured by PET because of decoupling between I-124 and the drug substrate. Once the I-124-labeled anti-VEGF agent exits the eye and becomes absorbed into the bloodstream, an uncertain proportion of I-124 decouples from its substrate and becomes sequestered by the thyroid gland, reducing the measured radioactivity in the peripheral organs. Since there were no significant differences found in the thyroid at any time point between the three agents, the amount of I-124 decoupling in the serum is likely to be proportional among the studied drugs. Within the vitreous cavity, anti-VEGF agents are not known to be metabolized, and the amount of decoupling is likely to be small. The clearance half-lives of previously reported intravitreal I-124 bevacizumab and I-124 ranibizumab measured by radioactive emission have compared favorably to pharmacokinetic reports using immunoassay methods in a similar rabbit model.[6–7] Future studies are needed to quantify the proportion of I-124 that decouples from the drug substrate in the serum, and to perhaps mathematically factor the decoupled proportion of I-124 into the radioactivity measurements for each of the studied organs. Second, the weight and size of an owl monkey is much smaller than that of an adult. The vitreous volume of the adult owl monkey varies between 2.0 and 2.5 mL as compared to approximately 4.5 mL in adult humans.[42] These animals also have much smaller serum compartments than adult humans, thus increasing their systemic exposure to humanly dosed intravitreal drugs. The blood and plasma volumes in owl monkeys are estimated to be 70 and 35 mL as compared to approximately 5 and 2.6 L in human adults.[43–45] However, the liquefied vitreous found in this primate model may better simulate the intravitreal pharmacokinetic properties found in elderly adults with posterior vitreous detachment. Further-

more, the weight of an owl monkey and the size of its eye closely simulate those of a premature infant with ROP, and the smaller serum size in the owl monkey model may more accurately represent the serum pharmacokinetic properties and biodistribution of intravitreally placed agents in these patients. Third, the use of a comparative methodology such as ELISA would have helped to verify serum measurements the radioactive decay of positron-emitting radionuclides is an inherently random process.[46] Unfortunately, ELISA serum assay analysis was not available at our institution during the course of this project. Finally, studies with larger numbers of subjects per agent may further delineate the intravitreal pharmacokinetic patterns, serum characteristics, and biodistribution uptakes of these agents, and may help to clarify whether or not the female–male differences in intravitreal retention rates of these drugs found in this investigation are significant.

In conclusion, our described methodology offers a novel approach for studying biodistribution and pharmacokinetic properties of radiolabeled intravitreally placed therapeutic agents by serial PET/CT imaging of the subject. I-124 bevacizumab had the longest intravitreal retention time and I-124 aflibercept the shortest. All three agents were found to be cleared through both the renal and mononuclear phagocytic systems. I-124 ranibizumab was rapidly cleared from the circulation, while I-124 bevacizumab had significantly higher and prolonged levels in the serum, heart, liver, and distal femur bones when compared to both I-124 ranibizumab and I-124 aflibercept.

Acknowledgments

The authors thank Valerie Bergdall, DVM, and Dondrae Coble, DVM, for their veterinary guidance and support throughout the study.

Presented in part at the Club Jules Gonin XXXth Meeting, Bordeaux, France, July 2016.

Supported in part by the Macular Degeneration Research Fund from the Department of Ophthalmology & Vision Science, University of Arizona Medical Center and Lions Clubs International.

Disclosure: **J.B. Christoforidis**, None; **K. Briley**, None; **K. Binzel**, None; **P. Bhatia**, None; **L. Wei**, None; **K. Kumar**, None; **M.V. Knopp**, None

References

1. Campbell RJ, Bronskill SE, Bell CM, et al. Rapid expansion of intravitreal drug injection procedures, 2000 to 2008: a population-based analysis. *Arch Ophthalmol*. 2010;128:359–362.
2. Williams GA. Intravitreal injections: health policy implications. *Rev Ophthalmol*. 2014;21:62–64.
3. Christoforidis JB, Carlton MM, Knopp MV, Hinkle GH. PET/CT imaging of I-124 radiolabeled bevacizumab and ranibizumab after intravitreal injection in a rabbit model. *Invest Ophthalmol Vis Sci*. 2011;52:5899–5903.
4. Christoforidis JB, Williams MM, Kothandaraman S, Kumar K, Epitropoulos FM, Knopp MV. Anatomic and pharmacokinetic properties of intravitreal I-124-aflibercept in a rabbit model using PET/CT. *Curr Eye Res*. 2012;37:1171–1174.
5. Christoforidis JB, Hinkle GH, Wang J, et al. Pharmacokinetic properties of intravitreally placed I-124 radiolabeled bevacizumab and ranibizumab after vitrectomy and lensectomy in a rabbit model. *Retina*. 2013;33:946–952.
6. Bakri SJ, Snyder MR, Reid JM, Pulido JS, Singh RJ. Pharmacokinetics of intravitreal bevacizumab (Avastin). *Ophthalmology*. 2007;114:855–859.
7. Bakri SJ, Snyder MR, Reid JM, Pulido JS, Ezzat MK, Singh RJ. Pharmacokinetics of intravitreal ranibizumab (Lucentis). *Ophthalmology*. 2007;114:2179–2182.
8. Belov VV, Bonab AA, Fischman AJ, Heartlein M, Calias P, Papisov MI. Iodine-124 as a label for pharmacological PET imaging. *Mol Pharm*. 2011;6:736–747.
9. Stafford JH, Hao G, Best AM, Sun X, Thorpe PE. Highly specific PET imaging of prostate tumors in mice with an iodine-124-labeled antibody fragment that targets phosphatidylserine. *PLoS One*. 2013;8:e84864.
10. O'Donoghue JA, Guillem JG, Schoder H, et al. Pilot study of PET imaging of ^{124}I-iodoazomycin galactopyranoside (IAZGP), a putative hypoxia imaging agent, in patients with colorectal cancer and head and neck cancer. *EJNMMI Res*. 2013;3:42.
11. Zou P, Povoski SP, Hall NC, et al. ^{124}I-HuCC49deltaC$_H$2 for TAG-72 antigen-directed positron emission tomography (PET) imaging of LS174T colon adenocarcinoma tumor implants in xenograft mice: preliminary results. *World J Surg Oncol*. 2010;8:65.
12. Park SJ, Choi Y, Na YM, et al. Intraocular pharmacokinetics of intravitreal aflibercept (Eylea) in a rabbit model. *Invest Ophthalmol Vis Sci*. 2016;57:2612–2617.
13. Chakrabarti B, Hultsch E. Owl monkey vitreous: a novel model for hyaluronic acid structural studies. *Biochem Biophys Res Commun*. 1976;71:1189–1193.
14. Niwa Y, Kakinoki M, Sawada T, Wang X, Ohji M. Ranibizumab and aflibercept: intraocular pharmacokinetics and their effects on aqueous VEGF level in vitrectomized and non-vitrectomized macaque eyes. *Invest Ophthalmol Vis Sci*. 2015;56:6501–6505.
15. Avery RL, Castellarin AA, Steinle NC, et al. Systemic pharmacokinetics and pharmacodynamics of intravitreal aflibercept, bevacizumab, and ranibizumab. *Retina*. 2017;37:1847–1858.
16. Avery RL, Castellarin AA, Steinle NC, et al. Systemic pharmacokinetics following intravitreal injections of ranibizumab, bevacizumab or aflibercept in patients with neovascular AMD. *Br J Ophthalmol*. 2014;98:1636–1641.
17. Zhang Y, Yao Z, Kaila N, et al. Pharmacokinetics of ranibizumab after intravitreal administration in patients with retinal vein occlusion or diabetic macular edema. *Ophthalmology*. 2014;21:2237–2246.
18. Gaudreault J, Fei D, Beyer JC, et al. Pharmacokinetics and retinal distribution of ranibizumab, a humanized antibody fragment directed against VEGF-A, following intravitreal administration in rabbits. *Retina*. 2007;27:1260–1266.
19. Gu X, Yu X, Dai H. Intravitreal injection of ranibizumab for treatment of age-related macular degeneration: effects on serum VEGF concentration. *Curr Eye Res*. 2014;39:518–521.
20. Wang X, Sawada T, Sawada O, Saishin Y, Liu P, Ohji M. Serum and plasma vascular endothelial growth factor concentrations before and after intravitreal injection of aflibercept or ranibizumab for age-related macular degeneration. *Am J Ophthalmol*. 2014;158:738–744.
21. Wu WC, Shih CP, Lien R, et al. Serum vascular endothelial growth factor after bevacizumab or ranibizumab treatment for retinopathy of prematurity. *Retina*. 2017;37:694–701.
22. Zhou Y, Jiang Y, Bai Y, Wen J, Chen L. Vascular endothelial growth factor plasma levels before and after treatment of retinopathy of prematurity with ranibizumab. *Graefes Arch Clin Exp Ophthalmol*. 2016;254:31–36.
23. Kong L, Bhatt AR, Demny AB, et al. Pharmacokinetics of bevacizumab and its effects on serum VEGF and IGF-1 in infants with retinopathy of prematurity. *Invest Ophthalmol Vis Sci*. 2015;56:956–961.
24. Sato T, Wada K, Arahori H, et al. Serum concentrations of bevacizumab (avastin) and vascular endothelial growth factor

in infants with retinopathy of prematurity. *Am J Ophthalmol*. 2012;153:327–333.

25. Dithmer M, Hattermann K, Pomarius P, et al. The role of Fc-receptors in the uptake and transport of therapeutic antibodies in the retinal pigment epithelium. *Exp Eye Res*. 2016;145:187–205.
26. Deissler HL, Lang GK, Lang GE. Internalization of bevacizumab by retinal endothelial cells and its intracellular fate: evidence for an involvement of the neonatal Fc receptor. *Exp Eye Res*. 2016;143:49–59.
27. Tschulakow A, Christner S, Julien S, Ludinsky M, van der Giet M, Schraermeyer U. Effects of a single intravitreal injection of aflibercept and ranibizumab on glomeruli of monkeys. *PLoS One*. 2014;9:e113701.
28. Shah MA, Ilson D, Kelsen DP. Thromboembolic events in gastric cancer: high incidence in patients receiving irinotecan- and bevacizumab-based therapy. *J Clin Oncol*. 2005;23:2574–2576.
29. Lordick F, Neinitz H, Thelsen J, Sendler A, Sarbia M. Increased risk of ischemic bowel complications during treatment with bevacizumab after pelvic irradiation: report of three cases. *Int J Radiat Oncol Biol Phys*. 2006;64:1295–1298.
30. Curtis LH, Hammill BG, Schulman KA, Cousins SW. Risks of mortality, myocardial infarction, bleeding, and stroke associated with therapies for age-related macular degeneration. *Arch Ophthalmol*. 2010;128:1273–1279.
31. Gordon CR, Rojavin Y, Patel M, et al. A review on bevacizumab and surgical wound healing: an important warning to all surgeons. *Ann Plast Surg*. 2009;62:707–709.
32. Zawacki WJ, Walker TG, DeVasher E, et al. Wound dehiscence or failure to heal following venous access port placement in patients receiving bevacizumab therapy. *J Vasc Interv Radiol*. 2009;20:624–627.
33. Scappaticci FA, Fehrenbacher L, Cartwright T, et al. Surgical wound healing complications in metastatic colorectal cancer patients treated with bevacizumab. *J Surg Oncol*. 2005;91:173–180.
34. Avery RL. What is the evidence for systemic effects of intravitreal anti-VEGF agents, and should we be concerned? *Br J Ophthalmol*. 2014;98(suppl 1):i7–i10.
35. Martin DF, Maguire MG, Fine SL, et al.; for the Comparison of Age-related Macular Degeneration Treatments Trials (CATT) Research Group. Ranibizumab and bevacizumab for treatment of neovascular age-related macular degeneration: two-year results. *Ophthalmology*. 2012;119:1388–1398.
36. Chakravarthy U, Harding SP, Rogers CA, et al. Alternative treatments to inhibit VEGF in age-related choroidal neovascularization: 2 year findings of the IVAN randomized controlled trial. *Lancet*. 2013;382:1258–1267.
37. Christoforidis JB, Wang J, Jiang A, et al. The effect of intravitreal bevacizumab and ranibizumab on cutaneous tensile strength during wound healing. *Clin Ophthalmol*. 2013;7:185–191.
38. Schrijvers BF, Flyvbjerg A, De Vriese AS. The role of vascular endothelial growth factor (VEGF) in renal pathophysiology. *Kidney Int*. 2004;65:2003–2017.
39. Pelle G, Shweke N, Duong Van Huyen JP, et al. Systemic and kidney toxicity of intraocular administration of vascular endothelial growth factor inhibitors. *Am J Kidney Dis*. 2011;57:756–759.
40. Cheungpasitporn W, Chebib FT, Cornell LD, et al. Intravitreal antivascular endothelial growth factor therapy may induce proteinuria and antibody mediated injury in renal allografts. *Transplantation*. 2015;99:2382–2386.
41. Georgalas I, Papaconstantinou D, Papadopoulos K, Pagoulatos D, Karagiannis D, Koutsandrea C. Renal injury following intravitreal anti-VEGF administration in diabetic patients with proliferative diabetic retinopathy and chronic kidney disease–a possible side effect? *Curr Drug Saf*. 2014;9:156–158.
42. Osterlin S, Balazs E. Macromolecular composition and fine structure of the vitreous in the owl monkey. *Exp Eye Res*. 1968;7:534–545.
43. Murphy KL, Baxter MB, Flecknell PA. Anesthesia and analgesia in nonhuman primates. In: Abee C, Mansfield K, Tardif S, Morris T, eds. *Nonhuman Primates in Biomedical Research*. London: Elsevier/Academic Press; 2012:427.
44. Malaga CA, Weller RE, Buschbom RI, Ragan HA. Hematology of the wild caught karyotype 1 owl monkey (Aotus nancymai). *Lab Anim Sci*. 1990:40:204–206.
45. Davy KP, Seals DR. Total blood volume in healthy young and older men. *J Appl Physiol*. 1990;76:2059–2062.
46. Watson CC, Casey ME, Bendriem B, et al. Optimizing injected dose in clinical PET by accurately modeling the counting-rate response functions specific to individual patient scans. *J Nucl Med*. 2005;46:1825–1834.

Investigative Ophthalmology & Visual Science